Orthogonal genome-wide screens of bat cells identify MTHFD1 as a target of broad antiviral therapy

Danielle E. Anderson[a,1,2], Jin Cui[b,1], Qian Ye[b,1], Baoying Huang[c,1], Ya Tan[b], Chao Jiang[b], Wenhong Zu[b], Jing Gong[b], Weiqiang Liu[d], So Young Kim[e], Biao Guo Yan[a], Kristmundur Sigmundsson[f], Xiao Fang Lim[a], Fei Ye[c], Peihua Niu[c], Aaron T. Irving[g], Haoyu Zhang[h], Yefeng Tang[h], Xuming Zhou[d], Yu Wang[i], Wenjie Tan[c], Lin-Fa Wang[a,3], and Xu Tan[b,3]

[a]Programme in Emerging Infectious Diseases, Duke–National University of Singapore Medical School, 169857 Singapore, Singapore; [b]MOE Key Laboratory of Bioorganic Phosphorus Chemistry & Chemical Biology, Beijing Advanced Innovation Center for Structural Biology, School of Pharmaceutical Sciences, Tsinghua-Peking Center for Life Sciences, Center for Infectious Disease Research, School of Medicine, Tsinghua University, 100084 Beijing, China; [c]National Health Commission Key Laboratory of Biosafety, Ministry of Health, National Institute for Viral Disease Control and Prevention, Chinese Center for Disease Control and Prevention, 102206 Beijing, China; [d]Key Laboratory of Animal Ecology and Conservation Biology, Institute of Zoology, Chinese Academy of Sciences, 100101 Beijing, China; [e]Department of Molecular Genetics and Microbiology, Duke University, Durham, NC 27708; [f]Programme in Cardiovascular & Metabolic Disorders, Duke–National University of Singapore Medical School, 169857 Singapore, Singapore; [g]Zhejiang University–University of Edinburgh Institute, Zhejiang University School of Medicine, 310058 Haining, China; [h]School of Pharmaceutical Sciences, Tsinghua University, 100084 Beijing, China; and [i]College of Life Sciences and Oceanography, Shenzhen University, 518071 Shenzhen, China

Edited by Shizuo Akira, Osaka Daigaku, Osaka, Japan, and approved August 16, 2021 (received for review March 16, 2021)

Bats are responsible for the zoonotic transmission of several major viral diseases, including those leading to the 2003 SARS outbreak and likely the ongoing COVID-19 pandemic. While comparative genomics studies have revealed characteristic adaptations of the bat innate immune system, functional genomic studies are urgently needed to provide a foundation for the molecular dissection of the viral tolerance in bats. Here we report the establishment of genome-wide RNA interference (RNAi) and CRISPR libraries for the screening of the model megabat, *Pteropus alecto*. We used the complementary RNAi and CRISPR libraries to interrogate *P. alecto* cells for infection with two different viruses: mumps virus and influenza A virus, respectively. Independent screening results converged on the endocytosis pathway and the protein secretory pathway as required for both viral infections. Additionally, we revealed a general dependence of the C1-tetrahydrofolate synthase gene, MTHFD1, for viral replication in bat cells and human cells. The MTHFD1 inhibitor, carolacton, potently blocked replication of several RNA viruses, including SARS-CoV-2. We also discovered that bats have lower expression levels of MTHFD1 than humans. Our studies provide a resource for systematic inquiry into the genetic underpinnings of bat biology and a potential target for developing broad-spectrum antiviral therapy.

bat | CRISPR | RNAi | antiviral therapy

As the only mammal capable of sustained flight, bats possess several unique behavioral and physiological characteristics. Bats are well known for their ability to harbor deadly viruses, causing the outbreaks of Ebola (1), SARS (2), Henipavirus (3), Middle East respiratory syndrome (4), and probably COVID-19 (5, 6). Bats are widely considered the largest reservoir of numerous virus species but are resilient to the diseases associated with these viruses (7, 8). How bats tolerate infection with these viruses is of intense interest due to the scientific and public health relevance. Comparative genomics studies have revealed several genetic adaptions underlying this tolerance of viral infections. For example, the DNA damage checkpoint pathway and the NF-κB pathway are known to be positively selected in the bat genomes (9). In addition, in the type I interferon gene family, the MHC class I genes and natural killer cell receptor family have been reported to be highly expanded in the bat genomes (10). These studies provide evidence to support the hypothesis that bats have evolved a highly specific genetic configuration, especially in the innate immunity pathways. A major caveat is the lack of systematic examination of the functions of these genes due to shortage of functional genomic tools for bat research.

CRISPR and RNA interference (RNAi) technologies have enabled genome-wide interrogation of gene functions for a variety of cell types, yielding an unprecedented wealth of information revealing the complexity of biological processes (11, 12). This is especially true in the field of virus–host interactions, where a plethora of host factors have been identified for a variety of viruses (13–15). Both technologies have advantages and disadvantages and provide complementary approaches to achieve comprehensive genetic perturbations (16–18). CRISPR permits complete knockout of a gene, and thus affords generation of a truly null genotype. A caveat is that the lethality associated with knockout of essential genes prevents functional parsing of these genes in different biological processes. In addition, CRISPR screens are usually used in a pool-based format that requires the generation of stable cell lines through long-term culturing. Based on previous studies, CRISPR screens demonstrated excellent specificity but limited sensitivity (17). In contrast, small-interfering

Significance

We established a genome-wide CRISPR library and a genome-wide RNA interference library for a bat species and performed two genetic screens to uncover host factors of bat cells involved in virus infections. Although the viruses and methodologies used were different in the two screens, we identified one common protein, MTHFD1, as a broad-spectrum host factor. Further studies show that the MTHFD1 inhibitor, carolacton, can potently inhibit a variety of viruses, including SARS-CoV-2. We provide a resource for studying the functional genomics of bat biology.

Author contributions: D.E.A., J.C., L.-F.W., and X.T. designed research; D.E.A., J.C., Q.Y., B.H., Y. Tan, C.J., B.G.Y., K.S., X.F.L., F.Y., P.N., and W.T. performed research; A.T.I., H.Z., Y. Tang, and Y.W. contributed new reagents/analytic tools; D.E.A., Q.Y., B.H., Y. Tan, W.Z., J.G., W.L., S.Y.K., B.G.Y., K.S., X.F.L., F.Y., P.N., X.Z., W.T., L.-F.W., and X.T. analyzed data; and D.E.A., S.Y.K., L.-F.W., and X.T. wrote the paper.

The authors declare no competing interest.

This article is a PNAS Direct Submission.

[1]D.E.A., J.C., Q.Y., and B.H. contributed equally to this work.

[2]Present address: Department of Microbiology and Immunology, The Peter Doherty Institute for Infection and Immunity, University of Melbourne, Melbourne, VIC 3000, Australia.

[3]To whom correspondence may be addressed. Email: linfa.wang@duke-nus.edu.sg or xutan@tsinghua.edu.cn.

This article contains supporting information online at https://www.pnas.org/lookup/suppl/doi:10.1073/pnas.2104759118/-/DCSupplemental.

Published September 20, 2021.

RNA (siRNA) screen relies on temporary knockdown of genes in an individual well format, a methodology suited for examining short-term phenotypic changes. Due to the transient nature of the assay, cells in siRNA screens can tolerate growth defects due to gene knockdown and can elucidate hypomorphic phenotypes induced by siRNAs with varying degrees of knockdown.

In general, RNAi screens allow comprehensive identification of genes in a biological process at the cost of more false positives due to pervasive off-target effects (17). To fully realize the power of CRISPR and RNAi technology as complementary strategies to interrogate gene function in bats, we developed a pool-based CRISPR library and a plate-based siRNA library for the whole genome of the model megabat *Pteropus alecto*. We analyzed two viruses, influenza A virus (IAV) and mumps virus (MuV), using the CRISPR and RNAi libraries, respectively, in the hope of uncovering common host factors for different viruses. From these two screens, common pathways, such as the endocytosis pathway and protein secretory pathway, were identified, demonstrating conserved pathways between bats and other mammals in hosting viral infections. We extensively characterized a common host factor, MTHFD1, and identified this gene as a critical factor for viral replication in both bats and humans. We further show that MTHFD1 is a potential target for developing broad-spectrum antiviral drugs. The MTHFD1 inhibitor, carolacton, demonstrated broad antiviral activity against Zika virus (ZIKV), MuV, and importantly, SARS-CoV-2. In summary, we developed two orthogonal libraries for genome-wide loss-of-function screens in bats and demonstrated their utility in discovery of important host factors for viral infections.

Results

Design and Validation of Genome-Wide CRISPR Library of *P. alecto*. We designed and synthesized the CRISPR and RNAi libraries based on the genome of *P. alecto*. For the CRISPR library, we adopted the algorithm developed for the construction of the popular GeCKO (genome-scale CRISPR-Cas9 knockout) library to select single-guide RNAs (sgRNAs) (19). We designed 85,275 sgRNAs targeting 21,336 genes annotated in the *P. alecto* genome with 21,302 genes with 4 sgRNAs for each gene. The other 34 genes have 1 to 3 sgRNAs due to the constraints of the gene sequences for designing sgRNAs. Selection of sgRNAs was based on the calculations of off-target scores to lower potential off-target effects of the sgRNAs. We synthesized the sgRNA library in an array-based oligonucleotide library and cloned into the lentiGuide-Puro lentivirus expression vector (20). The sgRNAs designs were validated for 21 sgRNAs targeting 11 genes using T7E1 endonuclease cleavage assay or Western blot. We observed 90.5% of effectiveness in gene editing or gene knockdown, supporting the quality of the designed library (*SI Appendix*, Fig. S1).

CRISPR Screen Identified IAV Host Factors. We performed a CRISPR screen with IAV in PaKi cells to identify viral host factors (Fig. 1*A*). IAV was chosen for the screen because the virus induces rapid cell death in infected PaKi cells, which is beneficial for the selection of strong hits. PaKi cells stably expressing both Cas9 and sgRNA libraries were infected with the H1N1 PR8 strain of IAV, in duplicate. A high multiplicity-of-infection (MOI) was used and naïve PaKi cells all died before day 9 postinfection. Surviving cells were collected and sgRNA abundance was compared with mock-infected cells. The two replicates demonstrated a high correlation, indicating high reproducibility (*SI Appendix*, Fig. S2). Using the RIGER algorithm, we identified 21 host factors required for the viral infection or pathogenesis (21) (Fig. 1*B* and Dataset S1). Three of the top four hits belonged to the V-type proton ATPase subunits (ATP6V1B2, ATP6V1F, and ATP6V0D1), proteins involved in the acidification of endosomes and that have previously been previous identified as key host factors for influenza virus entry in in human cells (Fig. 1*B* and *SI Appendix*, Fig. S3) (22). Among the other hits were two genes, COPZ1 and SEC23B, involved in the protein secretory pathway, which is also known to be required for the replication of many viruses, including influenza virus and flaviviruses (Fig. 1*B*) (22–24). The enrichment of previously known host factors in the identified hits in the CRISPR screen validated our library and the screening methodology. To further validate the results, we used independent small-hairpin RNAs (shRNAs) to knock down three genes identified in the CRISPR screen—NTS, ARHGAP9, and NEU4—which were not previously reported to be associated with influenza infection. Knockdown of the three genes using shRNA decreased infection of IAV in PaKi cells, consistent with the CRISPR screen results (*SI Appendix*, Fig. S4). NTS and NEU4 knockdown also inhibited IAV infection in 293T cells (*SI Appendix*, Fig. S4).

RNAi Screen Results Converge with CRISPR Screen on Key Pathways. We performed an RNAi screen in PaKi cells independently from the CRISPR screen to identify host factors required for the replication of GFP-expressing MuV, a paramyxovirus, which infects PaKi cells and can be detected using high-throughput microscopy (25) (Fig. 1*C*). The screen was performed in a 96-well format with MuV expressing EGFP from an additional open reading frame (25). PaKi cells were infected 48 h after transfection with the siRNA library. High-content imaging was utilized to quantify the infection rate and total cell number in each well, the latter indicating cytotoxicity of the siRNA. Excluding siRNAs with significant cytotoxicity, we selected 45 host-dependency factors whose knockdown resulted in significantly reduced viral infection and 45 host-restriction factors whose knockdown promoted viral infection based on the *z*-score of infection rate (Fig. 1*D* and Dataset S2). Comparing these results with our previously published MuV screen in human cells, we found only one gene required for infection in both species, WDR43 (25). However, comparison of pathways identified from human and bat screens indicate a common dependence on cellular processes including protein transport, RNA processing, and translation (Dataset S3). We selected several genes for individual validation with more replicates to obtain a high validation rate (11 of 12 of host-dependency factors and 7 of 12 of the host-restriction factors validated with at least one siRNA) (*SI Appendix*, Fig. S5), supporting the reproducibility of our screening methodology.

Although there is only one gene overlap between the host factors identified in both CRISPR and RNAi screens, we observed that multiple genes from the endocytosis pathway and protein secretory pathway were identified in both screens, albeit represented by different genes (Fig. 1 *B* and *D*). For the endocytosis pathway, two genes encoding components of the clathrin complex, CLTA and CLTC, were among the top three hits (Fig. 1*D*). Four genes involved in the protein secretory—namely ARF1, ARF4, COPG1, and SEC61B—were identified (Fig. 1*D*). This is consistent with the concept that both IAV and MuV require the two pathways for viral replication. In addition, protein translation initiation, which was previously reported to be required for IAV infection (22), was also represented in the top hits by three genes: EIF3B, EIF3G, and EIF4A3. Conversely, the RNAi screen also revealed genes that restricted MuV infection in PaKi cells. Among the top hits were several known antiviral genes, TRIM39, TRIM43 (26), and NAMPT (27). Overall, we identified candidate genes that potentially play a role in viral infection in bats.

The two pathways identified by both a CRISPR screen and siRNA screen, endocytosis and protein secretion, have previously been implicated in the human host response to a number of viral pathogens (*SI Appendix*, Fig. S3) (13, 22, 24, 28–32). To validate the role of these pathways in the bat response to viral infection, we established PaKi stable cell lines expressing shRNAs targeting several hits from the two screens. Stable knockdown of

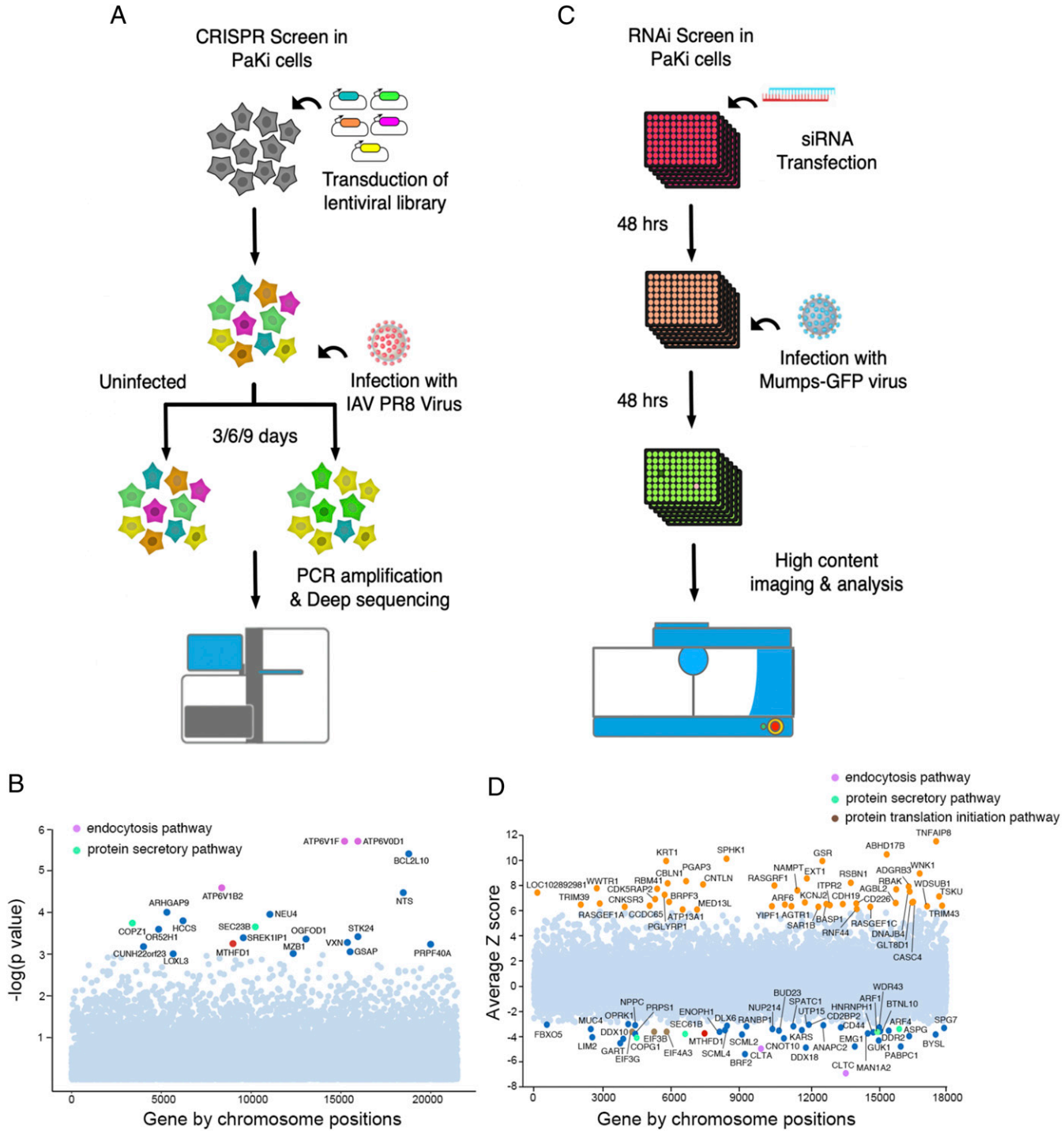

Fig. 1. Workflow and results of CRISPR and RNAi screens in PaKi cells. (*A*) For the CRISPR Cas9 knockout screen, PaKi cells stably expressing Cas9 were transduced with lentiviral sgRNA library targeting 21,300 genes of *P. alecto*. The transduced cells were selected with puromycin to generate the sgRNA cell library. Cells were infected with IAV PR8 strain (A/PuertoRico/8/1934) at a lethal dose or mock infected. The surviving cells were subjected to two more rounds of infection at day 3 and day 6 after the first infection. The surviving cells at day 9 after the first infection were harvested and the genomic DNA was extracted and amplified for the sgRNA region for analysis by deep sequencing. (*B*) The sgRNA abundance from sequencing was analyzed by the RIGER algorithm, the top hits representing host factors required for cell deaths from IAV infection are labeled. (*C*) For the siRNA screen, siRNAs targeting 18,328 genes of *P. alecto* were arrayed in 96-well plates. The siRNAs were reverse-transfected into PaKi cells and 48 h after transfection, the cells were infected with MuV. The percentage of infected cells was calculated at 48 hpi using high content imaging. (*D*) The siRNA targeted genes were ranked by robust *z*-score and wells with cytotoxicity were filtered out. Potential host factors or restriction factors are highlighted in the bottom and top, respectively.

three V-type proton ATPase subunits and two protein secretory pathway genes, SEC23B and SEC61B, led to a significant decrease of IAV infection in PaKi cells (*SI Appendix*, Fig. S6 *A*–*C*). In addition, the small-molecule inhibitor of V-type proton ATPase, bafilomycin A (*SI Appendix*, Fig. S6*D*), potently blocked IAV infection. Taken together, these results demonstrate that bat and

human cells share key genes and pathways in supporting viral infection.

MTHFD1 Is a Key Host Factor for a Broad Spectrum of RNA Viruses. MTHFD1 was identified as a host factor in both the CRISPR and RNAi screens (Fig. 1 *C* and *D*), which we validated by siRNA knockdown in the context of MuV infection (*SI Appendix*, Fig. S5). We validated the function in IAV replication in PaKi cells with two different sgRNAs targeting MTHFD1 (Fig. 2 *A* and *B*). Similarly, in HEK293T cells with MTHFD1 knocked out by two sgRNAs, IAV replication was inhibited, suggesting a conserved requirement for this gene by IAV in human cells (Fig. 2*C*). MTHFD1 knockdown significantly inhibits viral replication of MuV in PaKi cells (Fig. 2 *D* and *E*). The effect is similar to the knockdown of SEC61B, a well-studied host protein required for viral replication and a top hit in our RNAi screen (Fig. 2 *D* and *E*) (24). We additionally tested Melaka virus (PRV3M), a pteropine orthoreovirus that causes acute respiratory disease when transmitted from bats to humans (33). PRV3M replication was significantly reduced by MTHFD1 knockdown (Fig. 2 *E* and *F*). Infection of ZIKV, a member of the flavivirus family, was also inhibited by MTHFD1 knockdown using siRNA (Fig. 2*G*). Alternative knockdown with stable expression of two shRNAs validated the requirement of MTHFD1 for the replication of MuV and ZIKV (Fig. 2 *H*–*J*). Importantly, we also show that this inhibition is completely rescued by overexpression of MTHFD1 from a construct resistant to the shRNA, ruling out potential off-target effects (Fig. 2*K*).

MTHFD1's Formyl Tetrahydrofolate Synthetase Activity Is Essential for RNA Virus Replication. MTHFD1 is a trifunctional enzyme involved in the one carbon (C1) metabolism pathway, which is responsible for cellular production of purine, dTMP, and methyl groups (34). Two other enzymes involved in purine biosynthesis, GART and PRPS1, were also identified as hits in the PaKi siRNA screen, and pathway enrichment analysis identified multiple purine metabolism processes as essential for MuV infection (Dataset S3). MTHFD1 has three enzymatic functions, including dehydrogenase and cyclohydrolase activities encoded in the N-terminal domain and formyl tetrahydrofolate (Formyl THF) synthetase activity encoded in the C-terminal domain (Fig. 3 *A* and *B*). We first tested if virus entry into cells is infected by MTHFD1 knockdown. For IAV, ZIKV, and MuV, the entry step is not affected (*SI Appendix*, Fig. S7). We suspected that MTHFD1 knockdown would lead to the deficiency of cellular purine levels, thereby reducing RNA replication. We confirmed that MTHFD1 knockdown indeed caused decreased level cellular purine analogs (*SI Appendix*, Fig. S8). Supplementation of purine analogs, either hypoxanthine or inosine, almost completely rescued the replication of IAV and ZIKV in MTHFD1-knockout or -knockdown PaKi cells, as shown by both immunofluorescence staining and virus titration (Fig. 3 *C*–*E*).

In contrast, supplementation of methyl-group donor or thymidine had little effect on viral replication, evidence that it is the purine synthesis activity of MTHFD1 that is essential for the viral replication (Fig. 3*D*). To further pinpoint the enzymatic function of MTHFD1 in viral replication, we performed gene complementation experiments in an shRNA PaKi cell line with over 90% knockdown of MTHFD1 (Fig. 2*J*). The block of ZIKV replication in this cell line was completely rescued by overexpression of an shRNA-resistant MTHFD1 construct or a bat homolog (Fig. 3 *F* and *G*). Mutations of MTHFD1 that are known to disrupt its dehydrogenase and cyclohydrolase activities (D125A and R173C) (35, 36) did not affect this rescue (Fig. 3 *B* and *F*–*H*). However, mutations in the Formyl THF synthetase active site (F759A/W788A or FW/AA) (37) completely abolished this rescue, further supporting that the purine synthesis activity of MTHFD1 is an essential activity for viral replication (Fig. 3 *B* and *F*–*H*).

We observed a similar dependence on MTHFD1 function for IAV infection in HEK293T cells, a human kidney epithelial cell line (Fig. 3*I* and *SI Appendix*, Fig. S10). Time-course experiments demonstrated viral replication following MTHFD1 knockdown steadily decreased from 4 h postinfection (hpi) with IAV, consistent with an RNA replication defect (Fig. 3*J*). This defect in replication was completely rescued by supplementing the purine analog inosine in the media, supporting a conserved function of MTHFD1 in viral infection in bats and humans (Fig. 3 *I* and *K* and *SI Appendix*, Fig. S9). This is consistent with our metabolic measurement of purine analogs, which were reduced in MTHFD1-knockdown HEK293T cells but rescued by supplementing purine precursors (*SI Appendix*, Fig. S11). Levels of cytidine analogs (CMP/CDP/CTP) were also modestly reduced by MTHFD1 knockdown, likely due to an indirect effect of defect in purine synthesis.

MTHFD1 Inhibitor Carolacton Inhibits RNA Virus Replication. Carolacton, a natural product derived from bacteria, has recently been identified as a potent inhibitor of human MTHFD1 (38). Since the MTHFD1 sequence is conserved between human and *P. alecto* (*SI Appendix*, Fig. S12), we tested the effect of this compound on viral replication in PaKi cells. Carolacton inhibited ZIKV and MuV replication in PaKi cells in a dose-dependent manner (Fig. 4 *A*–*C*). The inhibition was achieved at doses with little effects on cellular metabolic activity, indicating low cytotoxicity (Fig. 4*A*). Mechanistically, this inhibition was completely rescued by supplementation of inosine, providing support that carolacton indeed exerts antiviral activities by inhibiting MTHFD1 (Fig. 4 *B* and *C*). We next tested the effect of carolacton on the infection of SARS-CoV-2 (39). The viral infection in Vero-E6 cells was effectively inhibited at submicromolar concentrations by carolacton (IC_{50} = 0.14 μM) (Fig. 4*D*). The cytotoxic effect is very moderate in comparison (Fig. 4*D*). We further tested the effect of carolacton on SARS-CoV-2 infection in Calu3 cells, a human lung adenocarcinoma cell line. Carolacton demonstrated consistently potent antiviral activity, with an IC_{50} of 50 nM (Fig. 4*E*). The half-cytotoxicity concentration (CC_{50}) is higher than 16 μM, giving a selectivity index (CC_{50}/IC_{50}) greater than 320 (Fig. 4*E*). Additionally, previous studies have shown that the cytotoxic concentrations of carolacton in a variety of human cancer cell lines are much higher than the antiviral concentration we observed here (38), supporting a wide therapeutic window of this compound in potential clinical applications.

Discussion

We developed a bat genome-wide RNAi and CRISPR library and performed two parallel screens with two different RNA viruses. Although the screening methodologies are different, we uncovered similar pathways essential for viral replication, namely the endocytosis pathway and protein secretory pathways. The different genes in these two pathways reflect the complementarity of the methodologies, with RNAi screen useful for revealing acute effects on viral infection and CRISPR screen for long-term effects on cell survival. Technical differences between screening methods, viral kinetics, sensitivity of the viruses to loss-of-function of genes and differences in genome coverage within the two libraries likely contributed to the different hits observed in our studies. This limited overlap between different screens is also observed among recent genome-wide CRISPR screens of SARS-CoV-2 host factors, as analyzed by Baggen et al. (40). Despite all of these technical and biological differences, an important common gene was uncovered. Both libraries provide valuable and complementary sources that meet the urgent need to address biological questions related to bats. Similar to human genomic libraries, the utility of these bat libraries in screening different bat cell types, especially those of the immune systems, would unveil more secrets of this enigmatic species.

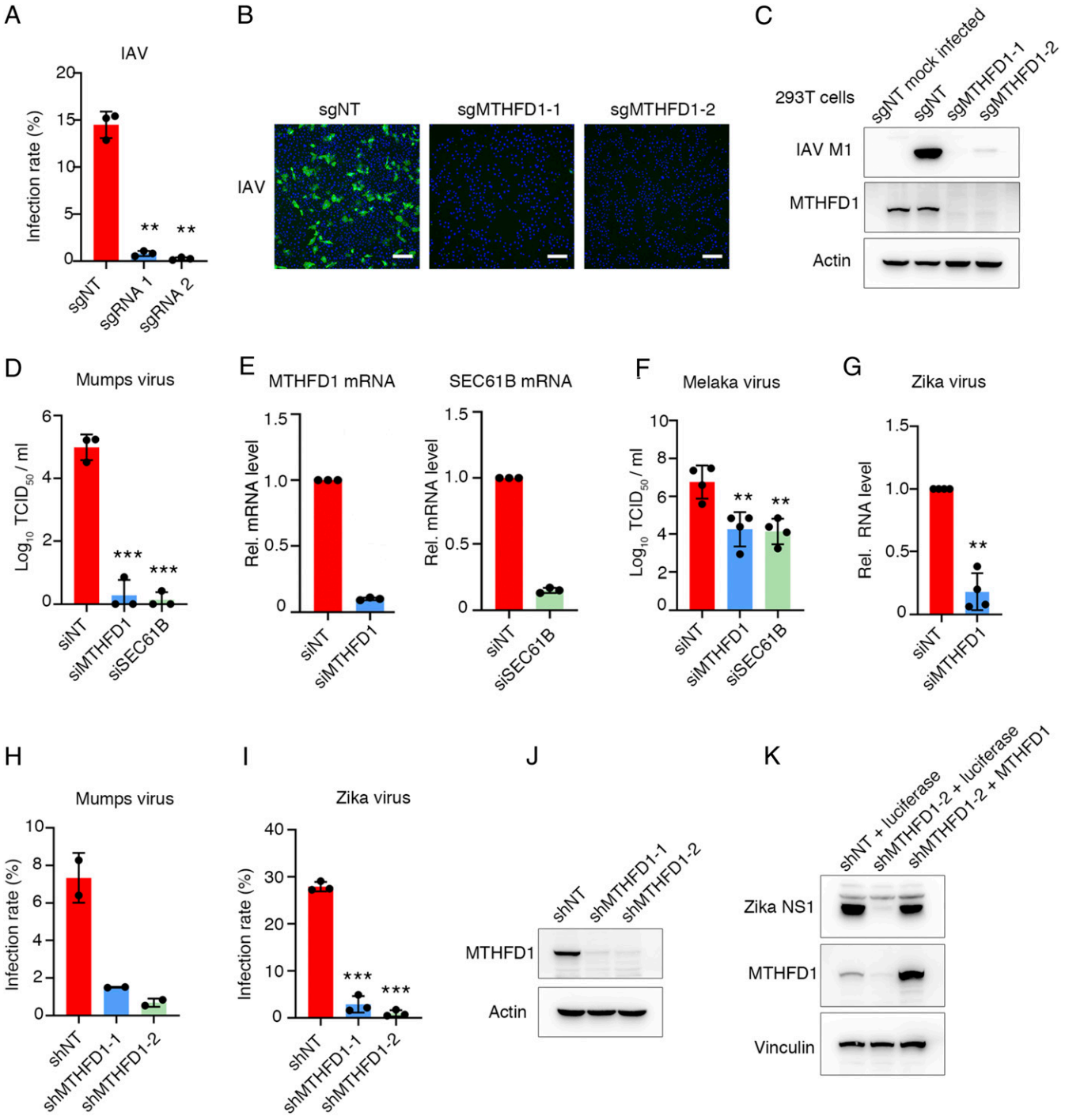

Fig. 2. MTHFD1 is a host factor for replication of multiple RNA viruses. (*A*) MTHFD1 knockout clonal PaKi cells were generated using two independent sgRNAs and infected with IAV for 12 h. The infection rates were quantified with immunofluorescent staining of HA. Data shown as the mean ± SD ($n = 3$). (*B*) Representative images from *A*. (Scale bar, 100 μm.) (*C*) MTHFD1 knockout 293T cells were generated from two independent sgRNAs and infected with IAV for another 12 h. The cells were collected and analyzed by Western blot. Data shown are representative of three independent experiments. (*D–F*) PaKi cells were transfected with nontarget control siRNA (siNT) or siRNAs targeting MTHFD1 and SEC61B followed by MuV (*D*) and Melaka virus (*F*) infection. The virus in the supernatant was titrated by limiting dilution. The knockdown efficiency was determined by real-time PCR and shown in *E*. For *D* and *E*, $n = 3$, and for *F*, $n = 4$. Data shown as the mean ± SD. (*G*) PaKi cells were transfected with siNT or siRNA targeting MTHFD1, and 48 h later the cells were infected with ZIKV. ZIKV RNA was measured by real-time PCR. $n = 4$. Data shown as the mean ± SD. (*H–J*) PaKi shRNA control cells (shNT) and shMTHFD1 cells were infected with MuV (*H*) or ZIKV (*I*) and the virus infection level was measured by immunofluorescence. For *H*, $n = 2$; for *I*, $n = 3$. Data shown as the mean ± SD. The shRNA knockdown efficiency was tested by Western blot as shown in *J*. Data shown are representative of three independent experiments. (*K*) Luciferase or an shRNA resistant MTHFD1 construct were stably expressed in shMTHFD1-2 PaKi cells, then the cells were infected with ZIKV. The rescue level of ZIKV was analyzed by Western blot. Data shown are representative of three independent experiments. For all bar graphs, the mean ± SD values are shown. $^{**}P < 0.01$, $^{***}P < 0.001$.

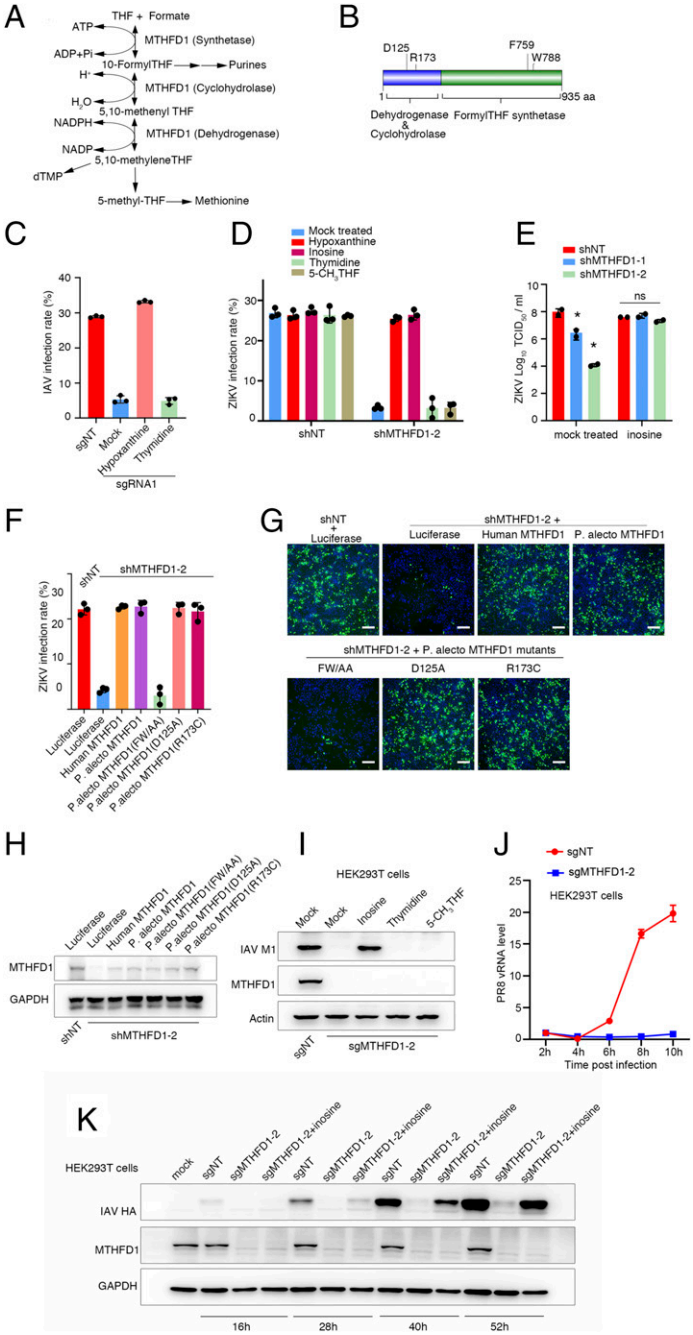

Fig. 3. MTHFD1's Formyl THF synthetase activity is essential for RNA virus replication. (*A*) MTHFD1 is a trifunctional enzyme in the one-carbon metabolism which is required for purine, dTMP, and methionine synthesis. (*B*) Domain structures and key amino acids of MTHFD1 with key residues for the three enzymatic functions indicated. (*C*) PaKi MTHFD1 knockout cells were infected with IAV with or without supplementation of hypoxanthine or thymidine for 12 h and the virus infection level was detected by immunofluorescence. Data shown as the mean ± SD ($n = 3$). (*D*) PaKi shMTHFD1-2 cells or control cells with a nontargeting shRNA were infected with ZIKV in regular medium or in medium supplemented with inosine, thymidine, or 5-CH_3THF. Data shown as the mean ± SD ($n = 3$). (*E*) PaKi shMTHFD1 cells were infected with ZIKV in regular medium or in medium supplemented with inosine. At 48 hpi, the virus in the supernatant was harvested and the titer was determined by limiting dilution in PaKi cells. Data shown as the mean ± SD ($n = 2$). (*F*) PaKi shMTHFD1-2 cells or control cells with a nontargeting shRNA were transfected with luciferase (negative control), human wild-type MTHFD1, bat wild-type MTHFD1, or bat MTHFD mutants, followed by ZIKV infection. The virus infection rate was measured by immunofluorescence. Data shown as the mean ± SD ($n = 3$). (*G*) Representative images from *F*. (Scale bars, 100 μm.) (*H*) Western blot of *F* showing the knockdown of MTHFD by shMTHFD1-2 and rescue by overexpression of human or bat MTHFD1 constructs. (*I*) HEK293T MTHFD1 knockout cells or control HEK293T cells with a nontargeting sgRNA (sgNT) were infected with IAV PR8 with or without the supplementation of inosine, thymidine, or 5-CH_3THF. At 12 hpi, the cells were collected and analyzed by Western blot. Data shown are representative of three independent experiments. (*J*) HEK293T MTHFD1 knockout cells (sgMTHFD1-2) or control cells (sgNT) were infected with IAV. The vRNA level was determined by real-time PCR at the indicated time points. The results are representative of three independent experiments. (*K*) HEK293T MTHFD1 knockout cells (sgMTHFD1-2) or control cells (sgNT) were transfected with plasmids expressing the IAV minigenome including polymerase subunits PB1, PB2, and PA, and nucleoprotein together with pPOLI-HA, which can transcribe the hemagglutinin vRNA of IAV. Inosine (100 μM) was added to MTHFD1 knockout cells before transfection. At 16, 28, 40, and 52 h posttransfection, the cells were collected and analyzed by Western blot. Data shown are representative of three independent experiments. For all bar graphs, the mean ± SD values are shown. *$P < 0.05$; ns, not significant.

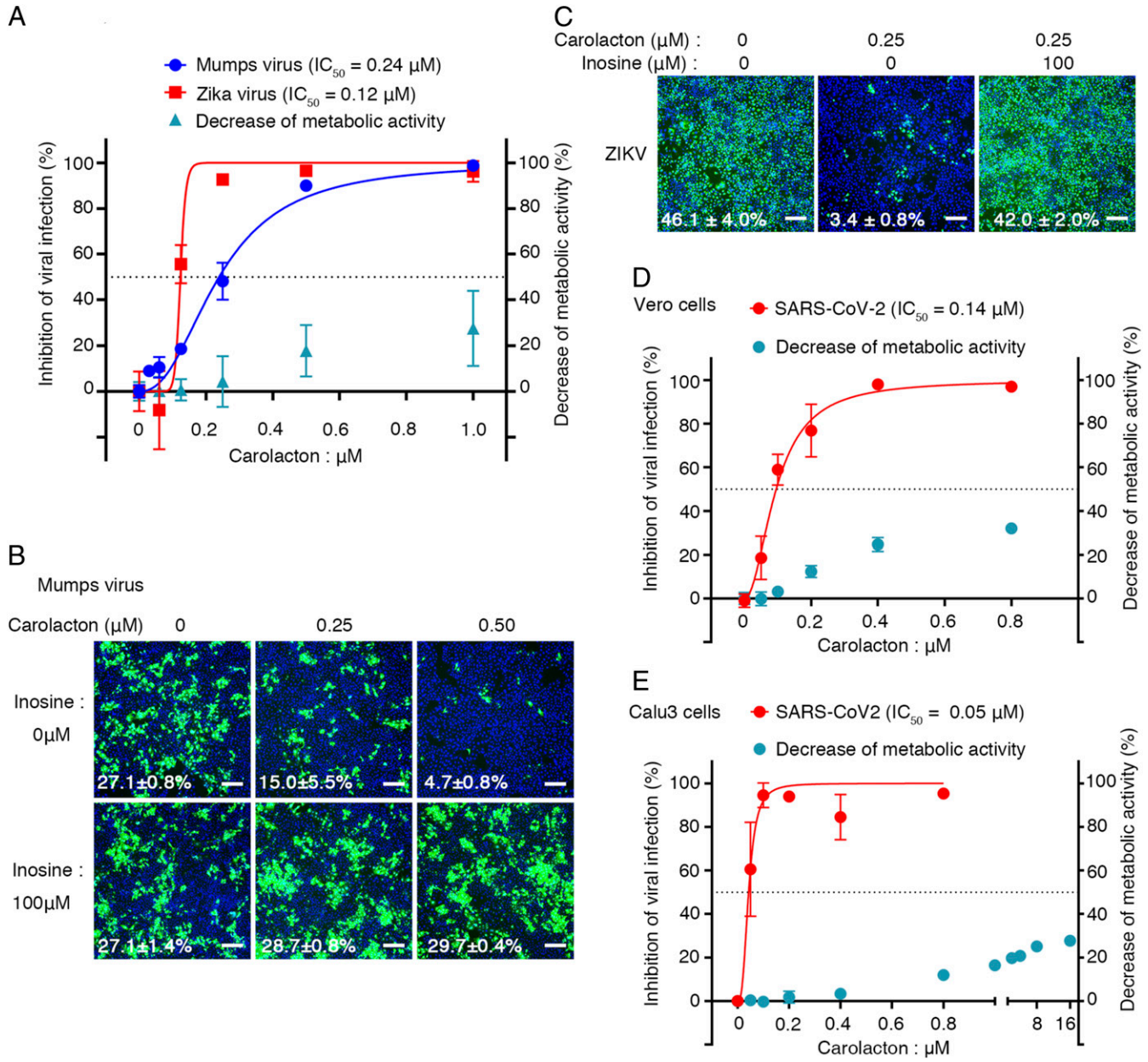

Fig. 4. MTHFD1 inhibitor carolacton can inhibit a number of RNA viruses including SARS-CoV-2. (*A*) PaKi cells were treated with different concentrations of carolacton and infected with ZIKV or MuV expressing EGFP. Virus infection levels were detected by immunofluorescence staining of Zika E protein or EGFP, respectively. The cell viability was measured by MTT assay. Data shown as the mean ± SD ($n = 3$). (*B*) PaKi cells were treated with carolacton and infected with MuV-EGFP with or without supplementing inosine. Representative images of immunofluorescence imaging of MuV-EGFP infected cells are shown. Infection rate shown as the mean ± SD ($n = 3$). (Scale bars: 100 μm.) (*C*) PaKi cells were treated with carolacton and infected with ZIKV with or without supplementing inosin. Representative images of immunofluorescence staining of ZIKV E protein are shown. Infection rate shown as the mean ± SD ($n = 3$). (Scale bars: 100 μm.) (*D* and *E*) Vero cells (*D*) or Calu3 cells (*E*) were treated with carolacton, and 1 h later infected with SARS-CoV-2. At 48 hpi, SARS-CoV-2 RNA in the supernatant was measured by real-time PCR. The cell viability was measured by MTT assay. Data shown as the mean ± SD ($n = 3$).

Both screens identified MTHFD1 as an essential viral host factor. MTHFD1 is a key enzyme in the C1 metabolism responsible for production of purine, dTMP, and methyl groups, the first two of which are building blocks for DNA and RNA synthesis. Interestingly, none of the previous RNAi or CRISPR screens using human cells has identified MTHFD1 as a host factor, which might be due to the different expression levels of PaKi cells and human cells. PaKi cells have significantly lower expression levels of MTHFD1 than a number of human cell lines, both at protein and mRNA levels (*SI Appendix*, Fig. S13 *A* and *B*). We examined transcriptomics data of *P. alecto* and human tissues. In both liver and spleen tissues, *P. alecto* has significantly lower level of MTHFD1 transcripts than human tissues (*SI Appendix*, Fig. S13*C*). This low expression level is also true for another bat species, *Eonycteris spelaea* (*SI Appendix*, Fig. S13*C*). Further analysis of three species indicated that the different expression levels might be related to the difference in the promoter regions between bats and humans, notably a lack of CCAAT box (41) in the promoter of two bat species (*SI Appendix*, Fig. S13*D*).

We show that MTHFD1 knockdown blocks replication of multiple RNA viruses, including IAV, MuV, Melaka virus, and

ZIKV. Although we mainly focused on RNA viruses, we also found the infection of HSV-1 is inhibited by the knockdown of MTHFD1 (*SI Appendix*, Fig. S14). Importantly, host cells have a higher tolerance for MTHFD1 inhibition than viruses, potentially providing a therapeutic window for targeting MTHFD1 with antiviral drugs. Virus infection converts the host cellular machinery into a factory to produce progeny viruses, which explains the vital dependence on MTHFD1. This is analogous to cancer cells' addiction to nononcogenic gene functions, such as many metabolic enzymes (42). Similar to the therapeutic targeting of these nononcogenic genes for developing cancer drugs, viral reliance on metabolic enzymes such as MTHFD1 could open doors to many new opportunities for developing broad-spectrum antiviral drugs (43). These drugs could be readily utilized in an outbreak situation and may greatly reduce the morbidity and mortality in an epidemic. Evidence that MTHFD1 inhibitor carolacton can suppress the replication of SARS-CoV-2 requires further investigation. We envision the functional genomics tools we outline here will be instrumental for further discoveries, leading to a better understanding the bat–virus interaction.

Materials and Methods

Cells and Virus. PaKi, Vero, and HEK293T cells were cultured in DMEM supplemented with 10% heat-inactivated FBS. Influenza H1N1 PR8 (A/Puerto Rico/8/1934) was propagated in embryonated eggs. Mumps virus was propagated in PaKi or Vero cells. The isolation and propagation of SARS-CoV-2 was reported earlier (39).

Genome-Wide CRISPR-Cas9 Knockout Screen. To design the CRISPR library, we adopted the algorithm developed for the construction of the popular GeCKO library to select sgRNAs (19). Cas9 stably expressed bat kidney-derived PaKi cells were transduced with lentivirus of sgRNA library (85,275 sgRNAs in total) targeting 21,336 genes in the genome of *P. alecto*. The transduced cells were selected with puromycin to generate the library cells. Then, at least 50 million sgRNA library cells were mock-infected (negative control) or changed with influenza A H1N1 PR8 strain (A/Puerto Rico/8/1934) at lethal doses (MOI = 5). This cell number ensures over 500-fold coverage for an average sgRNA. The surviving cells were subjected to two more rounds of infection. The final surviving cells were harvested to extract genomic DNA for deep-sequencing analysis. The screen was performed in duplicate and the sgRNA abundance was analyzed by the RIGER algorithm (21).

Deep-Sequencing Data Analysis. De-multiplexed reads were trimmed by Cutadapt (v1.18) (44) using 22-bp flanking sequences around the guide sequence. Trimmed reads were mapped to the index of bat sgRNA guide library using Bowtie2 (45). Samtools (46) (v1.9) was used to process the alignment files to retain perfectly mapped reads only, and a custom-made Python script was used to count the reads mapped to each sgRNA. The reads count of sgRNA for each condition were then normalized using DEseq2. The log2 ratio of counts between conditions were calculated. The log2 fold-change of reads counts of infected samples to mock-infected samples were then used as the input for RIGER algorithm, as previously described (RNAi Gene Enrichment Ranking, GENE-E) (21). The log-fold-change metric for ranking sgRNAs and the weighted sum method (weighted sum of first two ranks of sgRNAs for a gene) with 1×10^6 permutations were used to convert individual sgRNA to genes. In the output of RIGER analysis, a given gene was assigned a normalized enrichment score to give the ranked gene list. Hits were defined as those with *P* value smaller than 0.001.

siRNA Screen. For the siRNA screen, siRNAs targeting 18,328 genes of *P. alecto* were arrayed in the 96-well plates. The siRNAs were reverse-transfected into PaKi cells; 48 h later, the cells were infected with mumps virus. The virus infection level was calculated at 48 hpi by high content imaging (Operetta), as previously described (25). The screen was performed in duplicate. The siRNA targeted genes were ranked by robust *z*-scores, and the potential host factors (*z*-score < -3) or restriction factors (*z*-score > 6) were identified.

Validation of sgRNA. A single sgRNA was cloned into lentiGuide-puro (20) and packaged in lentivirus particles, which were transduced into Cas9 stably expressing PaKi cells, followed by puromycin and blasticidin selection. The clonal cells were generated by limiting dilution. The knockout or knockdown efficiencies were tested by Western blotting. To facilitate the growth of single clone MTHFD1 knockout cells, the cells were cultured with HT medium (DMEM supplemented with 10% FBS, 100 μM hypoxanthine, and 16 μM thymidine). Validated knockout cells were applied to virus infection assays. For MTHFD1 knockout cells, the HT was removed from the media 8 h before virus infection.

Validation of Hit Genes with shRNAs. Individual shRNAs were designed using the BLOCK-iT RNAi Designer (Thermo Fisher Scientific). The specificity was tested by BLAST (National Center for Biotechnology Information). The shRNA primers were synthesized as oligos listed in Table 1 and cloned into PLKO.1.

Western Blot. Cells were harvested and lysed in RIPA lysis buffer (Beyotime, P0013C) with a mixture of protease inhibitors (Biomake, B14001). Samples were applied to 10% or 12% SDS/PAGE gels (Bio-Rad) and transferred to PVDF membranes (Millipore). Membranes were blocked with 5% nonfat milk in PBS with 0.1% Tween 20 and then probed with primary antibodies. The following antibodies were used in this study: anti-MTHFD1 (Proteintech, 10794-1-AP), anti–β-actin (Easybio, BE0022), anti-PR8 M1 (Genetex, GTX125928-S), anti-HA (H1N1) (Genetex, GTX117951-S), anti-ZIKV NS1 (Genetex, GTX133307), antiflavivirus group antigen antibody (Millipore, MAB10216). The blots were developed by HRP reaction and imaged with a ProteinSimple FluorChem imaging system.

RNA Extraction and Real-Time PCR. Total RNA from cells was extracted using a HiPure Total RNA Mini Kit (Magen, R4111-03). The cDNA was generated by RevertAid RT Reverse Transcription Kit (Thermo Fisher Scientific, K1691). Influenza vRNA specific primer was used for vRNA transcription. The quantitative real-time PCR was performed with SYBR Green qPCR master mix (Vazyme, Q311-02) and data were analyzed by Bio-Rad CFX96 system. The primers for target genes were as follows:

Human GAPDH forward primer: 5′- ACAACTTTGGTATCGTGGAAGG-3′;

Human GAPDH reverse primer: 5′- GCCATCACGCCACAGTTTC-3′;

P. alecto ACTIN forward primer: 5′- GCCAGTCTACACCGTCTGCAG -3′;

P. alecto ACTIN reverse primer: 5′- CGTAGGAATCCTTCTGGCCCATG-3′;

P. alecto MTHFD1 forward primer: 5′- GGGAGCGACTGAAGAACCAAG-3′;

P. alecto MTHFD1 reverse primer: 5′- TCTTCAGCAGCCTTCAGCTTCAC-3′;

P. alecto SEC23B forward primer: 5′- GGCGTTTGGTGCTACTTTGG-3′;

P. alecto SEC23B reverse primer: 5′- TAGATGTGGGATCCAGGCCA-3′;

P. alecto SEC61B forward primer: 5′-GAAAAATGCCAGCTGCGGAA-3′;

P. alecto SEC61B reverse primer: 5′- GAACGAGTGTACTTGCCCCA-3′;

P. alecto GAPDH forward primer: 5′- ATACTTCTCATGGTTCACAC -3′;

P. alecto GAPDH reverse primer: 5′- TCATTGACCTCAACTACATG-3′;

P. alecto ATP6V1F forward primer: 5′- GGGCGGTATAGGGGAGCTTA-3′;

P. alecto ATP6V1F reverse primer: 5′-GTGCCGTACCATCTCTGCAA-3′;

P. alecto ATP6V1B2 forward primer: 5′-CTCGCTTGGCTCTAACCACA-3′;

P. alecto ATP6V1B2 reverse primer: 5′-ACATGTAGCCTGGGAAACCG-3′;

P. alecto ATP6V0D1 forward primer: 5′- GTGGTAGAGTTCCGCCACAT-3′;

P. alecto ATP6V0D1 reverse primer: 5′- CTCAAAGCTGCCTAGTGGGT-3′;

PR8 M1 forward primer: 5′- TTCTAACCGAGGTCGAAACGTACG-3′;

PR8 M1 reserve primer: 5′- ACAAAGCGTCTACGCTGCAG-3′;

PR8 vRNA reserve transcription primer: 5′-AGCRAAAGCAGG-3′;

ZIKV NS5 forward primer: 5′- GGTCAGCGTCCTCTCTAATAAACG-3′;

ZIKV NS5 reserve primer: 5′- GCACCCTAGTGTCCACTTTTTCC-3′.

Immunofluorescence. Virus-infected cells were fixed with 4% paraformaldehyde (PFA) for 10 min at room temperature, and permeated with 0.2% Triton X-100 for another 10 min at room temperature. Cells were washed with PBS three times and incubated with PR8 HA antibody or ZIKV E protein antibody for 2 h at room temperature or 4 °C overnight, then washed with PBS three times and incubated with second antibody conjugated with AF488

Table 1. shRNA sequences used in the study

shRNA	Direction	Sequence
shMTHFD1-1	Forward	5′-CCGGGCACATGGGAATTCCTCTACCCTCGAGGGTAGAGGAATTCCCATGTGCTTTTTG-3′
shMTHFD1-2	Reverse	5′-AATTCAAAAAGCACATGGGAATTCCTCTACCCTCGAGGGTAGAGGAATTCCCATGTGC-3′
shMTHFD1-3	Forward	5′-CCGGGCCTGCTGTCACTTAGGAAATCTCGAGATTTCCTAAGTGACAGCAGGCTTTTTG-3′
shMTHFD1-4	Reverse	5′-AATTCAAAAAGCCTGCTGTCACTTAGGAAATCTCGAGATTTCCTAAGTGACAGCAGGC-3′
shSEC23B-1	Forward	5′-CCGGGGAGATTCTTTCAACACTTCTCTCGAGAGAAGTGTTGAAAGAATCTCCTTTTTG-3′
shSEC23B-1	Reverse	5′-AATTCAAAAAGGAGATTCTTTCAACACTTCTCTCGAGAGAAGTGTTGAAAGAATCTCC-3′
shSEC23B-2	Forward	5′-CCGGGCAGGAACCATTGGTCCTTGTCTCGAGACAAGGACCAATGGTTCCTGCTTTTTG-3′
shSEC23B-2	Reverse	5′-AATTCAAAAAGCAGGAACCATTGGTCCTTGTCTCGAGACAAGGACCAATGGTTCCTGC-3′
shSEC61B-1	Forward	5′-CCGGGCTACATCCATCTGTCTATCACTCGAGTGATAGACAGATGGATGTAGCTTTTTG-3′
shSEC61B-1	Reverse	5′-AATTCAAAAAGCTACATCCATCTGTCTATCACTCGAGTGATAGACAGATGGATGTAGC-3′
shSEC61B-2	Forward	5′-CCGGGGTCCTTTGAGATCTCCATCGCTCGAGCGATGGAGATCTCAAAGGACCTTTTTG-3′
shSEC61B-2	Reverse	5′-AATTCAAAAAGGTCCTTTGAGATCTCCATCGCTCGAGCGATGGAGATCTCAAAGGACC-3′
shARHGAP9-1	Forward	5′-CCGGGCGTTGCTGCTGTGGATAAGACTCGAGTCTTATCCACAGCAGCAACGCTTTTTG-3′
shARHGAP9-1	Reverse	5′-AATTCAAAAAGCGTTGCTGCTGTGGATAAGACTCGAGTCTTATCCACAGCAGCAACGC-3′
shARHGAP9-2	Forward	5′-CCGGGCATTTGTGCAGGGTGATAACCTCGAGGTTATCACCCTGCACAAATGCTTTTTG-3′
shARHGAP9-2	Reverse	5′-AATTCAAAAAGCATTTGTGCAGGGTGATAACCTCGAGGTTATCACCCTGCACAAATGC-3′
shATP6V1F-1	Forward	5′-CCGGCATCCTCATCAACCAGTACATCTCGAGATGTACTGGTTGATGAGGATGTTTTTG-3′
shATP6V1F-1	Reverse	5′-AATTCAAAAACATCCTCATCAACCAGTACATCTCGAGATGTACTGGTTGATGAGGATG-3′
shATP6V1F-2	Forward	5′-CCGGTCAATGAGATCGAAGACACTTCTCGAGAAGTGTCTTCGATCTCATTGATTTTTG-3′
shATP6V1F-2	Reverse	5′-AATTCAAAAATCAATGAGATCGAAGACACTTCTCGAGAAGTGTCTTCGATCTCATTGA-3′
shATP6V1B2-1	Forward	5′-CCGGCGCCTCACATACAAGACAGTACTCGAGTACTGTCTTGTATGTGAGGCGTTTTTG-3′
shATP6V1B2-1	Reverse	5′-AATTCAAAAACGCCTCACATACAAGACAGTACTCGAGTACTGTCTTGTATGTGAGGCG-3′
shATP6V1B2-2	Forward	5′-CCGGCCGGTTCTTCAAATCTGACTTCTCGAGAAGTCAGATTTGAAGAACCGGTTTTTG-3′
shATP6V1B2-2	Reverse	5′-AATTCAAAAACCGGTTCTTCAAATCTGACTCTCGAGAAGTCAGATTTGAAGAACCGG-3′
shATP6V0D1-1	Forward	5′-CCGGGCTGAGCTCTACAATGCTATTCTCGAGAATAGCATTGTAGAGCTCAGCTTTTTG-3′
shATP6V0D1-1	Reverse	5′-AATTCAAAAAGCTGAGCTCTACAATGCTATTCTCGAGAATAGCATTGTAGAGCTCAGC-3′
shATP6V0D1-2	Forward	5′-CCGGGGACCGATTCTTTGAGCATGACTCGAGTCATGCTCAAAGAATCGGTCCTTTTTG-3′
shATP6V0D1-2	Reverse	5′-AATTCAAAAAGGACCGATTCTTTGAGCATGACTCGAGTCATGCTCAAAGAATCGGTCC-3′
shNEU4-1	Forward	5′-CCGGGCTTCTCCATGGAGAGTTGCACTCGAGTGCAACTCTCCATGGAGAAGCTTTTTG-3′
shNEU4-1	Reverse	5′-AATTCAAAAAGCTTCTCCATGGAGAGTTGCACTCGAGTGCAACTCTCCATGGAGAAGC-3′
shNEU4-2	Forward	5′-CCGGAGGTCTCCTACGAGGAGATTGCTCGAGCAATCTCCTCGTAGGAGACCTTTTTTG-3′
shNEU4-2	Reverse	5′-AATTCAAAAAAGGTCTCCTACGAGGAGATTGCTCGAGCAATCTCCTCGTAGGAGACCT-3′
shNTS-1	Forward	5′-CCGGGCATGATACTCCTGGCTTTCACTCGAGTGAAAGCCAGGAGTATCATGCTTTTTG-3′
shNTS-1	Reverse	5′-AATTCAAAAAGCATGATACTCCTGGCTTTCACTCGAGTGAAAGCCAGGAGTATCATGC-3′
shNTS-2	Forward	5′-CCGGGGAGTTAATTCAGGAAGATGTCTCGAGACATCTTCCTGAATTAACTCCTTTTTG-3′
shNTS-2	Reverse	5′-AATTCAAAAAGGAGTTAATTCAGGAAGATGTCTCGAGACATCTTCCTGAATTAACTCC-3′

(goat anti-mouse). The nuclei were stained with DAPI. Images were acquired with Cellomics ArrayScan VTI HCS (Thermo Fisher Scientific)

Virus Titration. Virus titers were determined by limiting dilution on PaKi cells (47).

Metabolomics. The Dionex Ultimate 3000 UPLC system was coupled to a TSQ Quantiva Ultra triple-quadrupole mass spectrometer (Thermo Fisher Scientific), equipped with a heated electrospray ionization probe. Extracts were separated by a synergi Hydro-RP column (2.0 × 100 mm, 2.5 μm; Phenomenex). A binary solvent system was used, in which mobile phase A consisted of 10 mM tributylamine adjusted with 15 mM acetic acid in water, and mobile phase B of methanol. This analysis used a 25-min gradient from 5 to 90% mobile B. Data acquired in selected reaction monitoring in negative-ion mode. The ion transitions were optimized using chemical standards. The resolution for Q1 and Q3 are both 0.7 full-width half maximum. The source parameters are as follows: spray voltage: 2,500 v; capillary temperature: 350 °C; heater temperature: 300 °C; sheath gas flow rate: 35; auxiliary gas flow rate: 10. Data analysis and quantitation were performed by the software Tracefinder 3.1.

Influenza Virus Minigenome Assay. Approximately 2×10^5 of HEK293T cells or MTHFD1 knockout HEK293T cells were plated into each well of 12-well plates and the knockout cells were cultured with HT (100 μM hypoxanthine and 16 μM thymidine; Gibco) medium. Then the cells were transfected with the plasmids expressing viral polymerase subunits PB1, PB2, and PA, and nucleoprotein, together with pPOLI–HA, transcribing hemagglutinin vRNA segment of A/WSN/33(H1N1) (WSN). At the time of transfection, HT was removed from the cells and supplied with fresh medium with or without supplementation of inosine (100 μM). The HA protein level was analyzed at 16, 28, 40, and 52 h posttransfection by Western blot.

SARS-CoV-2 Infection Assay. This experiment was performed in the BSL-3 laboratory at the Chinese Center for Disease Control and Prevention. Approximately 1×10^4 Vero cells were seeded each well in a 96-well plate 1 d before being treated with compounds for 1 h. Then SARS-CoV-2 (C-Tan-nCoV Wuhan strain 01) (39) was added to the cells at the titer of 100 $TCID_{50}$/100 μL. The media ware harvested at 48 hpi. RNA was extracted from the harvested media and qRT-PCR was performed to quantitate the viral RNA.

MTT Assay. MTT cell viability assay (Solarbio) was used to analyze cell viability according to the manufacturer's instructions. Briefly, 10 μL MTT (0.5%) mixed with 90 μL fresh medium was added into the well. The cells were incubated at 37 °C for 4 h, after the formazan crystals were formed, the medium was removed, and 110 μL DMSO was used to solubilize the formazan crystals. The absorbance at 490 nm was measured with a multimode plate reader Victor x5 (Perkin-Elmer).

Chemical Synthesis. Carolacton was synthesized following the procedure developed by the Goswami group (48), and the synthetic sample displayed identical spectroscopic data with the natural product.

Data Availability. All study data are included in the article and supporting information.

ACKNOWLEDGMENTS. We thank Jianzhong Xi for oligonucleotide synthesis; Rolf Muller and Chengzhang Fu for providing 0.2 mg carolacton as reference compound; and the Metabolomics Facility Center in National Protein Science Technology Center of Tsinghua University for metabolomics experiments.

X.T. was supported by the China National Funds for Excellent Young Scientists (31722030), the Beijing Advanced Innovation Center for Structural Biology, and the Tsinghua-Peking Joint Center for Life Sciences and the Spring Breeze Fund of Tsinghua University. X.T. and Y.W. were supported by the Science, Technology, and Innovation Committed of Shenzhen Municipality (Grant [2020] 295). D.E.A. and L.-F.W. were supported by Grants NRF2012NRF-CRP001-056 and NRF2016NRF-NSFC002-013 from the Singapore National Research Foundation. D.E.A. was supported by a National Medical Research Council Cooperative Basic Research Grant (NMRC/BNIG/2030/2015). Y. Tang was supported by Beijing Natural Science Foundation (M21011).

1. E. M. Leroy *et al*., Fruit bats as reservoirs of Ebola virus. *Nature* **438**, 575–576 (2005).
2. W. Li *et al*., Bats are natural reservoirs of SARS-like coronaviruses. *Science* **310**, 676–679 (2005).
3. B. A. Clayton, L. F. Wang, G. A. Marsh, Henipaviruses: An updated review focusing on the pteropid reservoir and features of transmission. *Zoonoses Public Health* **60**, 69–83 (2013).
4. H. A. Mohd, J. A. Al-Tawfiq, Z. A. Memish, Middle East respiratory syndrome coronavirus (MERS-CoV) origin and animal reservoir. *Virol. J.* **13**, 87 (2016).
5. F. Wu *et al*., A new coronavirus associated with human respiratory disease in China. *Nature* **579**, 265–269 (2020).
6. P. Zhou *et al*., A pneumonia outbreak associated with a new coronavirus of probable bat origin. *Nature* **579**, 270–273 (2020).
7. K. J. Olival *et al*., Host and viral traits predict zoonotic spillover from mammals. *Nature* **546**, 646–650 (2017).
8. L. F. Wang, D. E. Anderson, Viruses in bats and potential spillover to animals and humans. *Curr. Opin. Virol.* **34**, 79–89 (2019).
9. G. Zhang *et al*., Comparative analysis of bat genomes provides insight into the evolution of flight and immunity. *Science* **339**, 456–460 (2013).
10. S. S. Pavlovich *et al*., The Egyptian Rousette genome reveals unexpected features of bat antiviral immunity. *Cell* **173**, 1098–1110.e18 (2018).
11. S. Mohr, C. Bakal, N. Perrimon, Genomic screening with RNAi: Results and challenges. *Annu. Rev. Biochem.* **79**, 37–64 (2010).
12. O. Shalem, N. E. Sanjana, F. Zhang, High-throughput functional genomics using CRISPR-Cas9. *Nat. Rev. Genet.* **16**, 299–311 (2015).
13. W. M. McDougall, J. M. Perreira, E. C. Reynolds, A. L. Brass, CRISPR genetic screens to discover host-virus interactions. *Curr. Opin. Virol.* **29**, 87–100 (2018).
14. D. Panda, S. Cherry, Cell-based genomic screening: Elucidating virus-host interactions. *Curr. Opin. Virol.* **2**, 784–792 (2012).
15. A. S. Puschnik, K. Majzoub, Y. S. Ooi, J. E. Carette, A CRISPR toolbox to study virus-host interactions. *Nat. Rev. Microbiol.* **15**, 351–364 (2017).
16. A. Schuster *et al*., RNAi/CRISPR screens: From a pool to a valid hit. *Trends Biotechnol.* **37**, 38–55 (2019).
17. J. M. Perreira, P. Meraner, A. L. Brass, Functional genomic strategies for elucidating human-virus interactions: Will CRISPR knockout RNAi and haploid cells? *Adv. Virus Res.* **94**, 1–51 (2016).
18. J. Taylor, S. Woodcock, A perspective on the future of high-throughput RNAi screening: Will CRISPR cut out the competition or can RNAi help guide the way? *J. Biomol. Screen.* **20**, 1040–1051 (2015).
19. O. Shalem *et al*., Genome-scale CRISPR-Cas9 knockout screening in human cells. *Science* **343**, 84–87 (2014).
20. N. E. Sanjana, O. Shalem, F. Zhang, Improved vectors and genome-wide libraries for CRISPR screening. *Nat. Methods* **11**, 783–784 (2014).
21. B. Luo *et al*., Highly parallel identification of essential genes in cancer cells. *Proc. Natl. Acad. Sci. U.S.A.* **105**, 20380–20385 (2008).
22. T. Watanabe, S. Watanabe, Y. Kawaoka, Cellular networks involved in the influenza virus life cycle. *Cell Host Microbe* **7**, 427–439 (2010).
23. P. Zhu *et al*., Host cellular protein TRAPPC6AΔ interacts with influenza a virus M2 protein and regulates viral propagation by modulating M2 trafficking. *J. Virol.* **91**, e01757-16 (2016).
24. P. S. Shah *et al*., Comparative flavivirus-host protein interaction mapping reveals mechanisms of dengue and Zika virus pathogenesis. *Cell* **175**, 1931–1945 e1918 (2018).
25. D. E. Anderson *et al*., Comparative loss-of-function screens reveal ABCE1 as an essential cellular host factor for efficient translation of *Paramyxoviridae* and *Pneumoviridae*. *MBio* **10**, e00826-19 (2019).
26. M. van Gent, K. M. J. Sparrer, M. U. Gack, TRIM proteins and their roles in antiviral host defenses. *Annu. Rev. Virol.* **5**, 385–405 (2018).
27. J. W. Schoggins *et al*., A diverse range of gene products are effectors of the type I interferon antiviral response. *Nature* **472**, 481–485 (2011).
28. J. Han *et al*., Genome-wide CRISPR/Cas9 screen identifies host factors essential for influenza virus replication. *Cell Rep.* **23**, 596–607 (2018).
29. A. L. Brass *et al*., The IFITM proteins mediate cellular resistance to influenza A H1N1 virus, West Nile virus, and dengue virus. *Cell* **139**, 1243–1254 (2009).
30. R. König *et al*., Human host factors required for influenza virus replication. *Nature* **463**, 813–817 (2010).
31. A. Karlas *et al*., Genome-wide RNAi screen identifies human host factors crucial for influenza virus replication. *Nature* **463**, 818–822 (2010).
32. W. C. Su *et al*., Pooled RNAi screen identifies ubiquitin ligase Itch as crucial for influenza A virus release from the endosome during virus entry. *Proc. Natl. Acad. Sci. U.S.A.* **110**, 17516–17521 (2013).
33. K. B. Chua *et al*., A previously unknown reovirus of bat origin is associated with an acute respiratory disease in humans. *Proc. Natl. Acad. Sci. U.S.A.* **104**, 11424–11429 (2007).
34. G. S. Ducker, J. D. Rabinowitz, One-carbon metabolism in health and disease. *Cell Metab.* **25**, 27–42 (2017).
35. M. S. Field, E. Kamynina, D. Watkins, D. S. Rosenblatt, P. J. Stover, Human mutations in methylenetetrahydrofolate dehydrogenase 1 impair nuclear de novo thymidylate biosynthesis. *Proc. Natl. Acad. Sci. U.S.A.* **112**, 400–405 (2015).
36. S. Sundararajan, R. E. MacKenzie, Residues involved in the mechanism of the bifunctional methylenetetrahydrofolate dehydrogenase-cyclohydrolase: The roles of glutamine 100 and aspartate 125. *J. Biol. Chem.* **277**, 18703–18709 (2002).
37. L. R. Celeste *et al*., Mechanism of N10-formyltetrahydrofolate synthetase derived from complexes with intermediates and inhibitors. *Protein Sci.* **21**, 219–228 (2012).
38. C. Fu *et al*., The natural product carolacton inhibits folate-dependent C1 metabolism by targeting FolD/MTHFD. *Nat. Commun.* **8**, 1529 (2017).
39. N. Zhu *et al*.; China Novel Coronavirus Investigating and Research Team, A novel coronavirus from patients with pneumonia in China, 2019. *N. Engl. J. Med.* **382**, 727–733 (2020).
40. J. Baggen *et al*., Genome-wide CRISPR screening identifies TMEM106B as a proviral host factor for SARS-CoV-2. *Nat. Genet.* **53**, 435–444 (2021).
41. G. E. Martyn, K. G. R. Quinlan, M. Crossley, The regulation of human globin promoters by CCAAT box elements and the recruitment of NF-Y. *Biochim. Biophys. Acta. Gene Regul. Mech.* **1860**, 525–536 (2017).
42. J. Luo, N. L. Solimini, S. J. Elledge, Principles of cancer therapy: Oncogene and non-oncogene addiction. *Cell* **136**, 823–837 (2009).
43. R. M. Deans *et al*., Parallel shRNA and CRISPR-Cas9 screens enable antiviral drug target identification. *Nat. Chem. Biol.* **12**, 361–366 (2016).
44. M. Martin, Cutadapt removes adapter sequences from high-throughput sequencing reads. *EMBnet j* **17**, 10–12 (2011).
45. B. Langmead, S. L. Salzberg, Fast gapped-read alignment with Bowtie 2. *Nat. Methods* **9**, 357–359 (2012).
46. H. Li *et al*.; 1000 Genome Project Data Processing Subgroup, The sequence alignment/map format and SAMtools. *Bioinformatics* **25**, 2078–2079 (2009).
47. L. J. Reed, H. Muench, A simple method of estimating fifty percent endpoints. *Am. J. Hyg.* **27**, 493–497 (1938).
48. T. K. Kuilya, R. K. Goswami, Stereoselective total synthesis of carolacton. *Org. Lett.* **19**, 2366–2369 (2017).